

Interpretation of magnetophotoluminescence spectra of narrow-gap IV-VI semiconductors

R. Rupprecht and H. Pascher

Experimentalphysik I, Universität Bayreuth, D-95440 Bayreuth, Germany

(Received 13 June 1994)

In order to explain experimentally observed magnetophotoluminescence line shapes, theoretical models of interband recombination in the case of \mathbf{k} conservation as well as in case of violation of that selection rule have been developed for narrow-gap IV-VI semiconductors. The combined density of states and the individual densities of states of the conduction and the valence bands, respectively, as well as the occupation probabilities of these levels are taken into account. Modifications of the band structure due to many-particle effects (free carriers due to doping of the samples and photoexcited electrons and holes) are also included in the theoretical calculations of the luminescence line shapes. The spectral intensity distribution of the recombination radiation can be explained as spontaneous and stimulated emission of a homogeneous nonequilibrium electron-hole plasma. From least-squares fits to the experimentally observed photoluminescence line shapes, averaged plasma parameters can be deduced. Without an external magnetic field the unrenormalized single-particle band gap, its modifications due to exchange and correlation energy terms, the quasi-Fermi levels, and the effective temperature of the photoexcited carriers can be obtained. In addition, in the case of an external magnetic field one can determine the Dingle temperature and estimate the magnetic-field dependence of the renormalization of the band gap, if the band structure of the investigated material is known. Measurements of the photoluminescence have been performed at a lattice temperature of $T_L = 1.7$ K in a magnetic-field range of $B = 0-7$ T for a variety of IV-VI narrow-gap semiconductors. In the present paper we discuss the results obtained using $\text{Pb}_{1-x}\text{Eu}_x\text{Se}$ epitaxial films with Eu contents x of approximately 4%. The agreement between experimentally observed and calculated line shapes is excellent. However, due to the large number of plasma parameters entering the model, it seems difficult to determine the band structure of a semiconductor only using photoluminescence data.

I. INTRODUCTION

Photoluminescence is one of the most important experimental methods for the investigation of semiconductor materials. Of particular interest are IV-VI narrow-gap semiconductors,¹⁻⁵ due to their possible application as laser diodes operating in the midinfrared.

Interpretation of photoluminescence data requires a detailed understanding of the line shapes, including the effects of many-particle interactions (exchange and correlation energy terms), carrier heating by the exciting light, possible violation of momentum conservation, and onset of stimulated emission. Particularly with the sample held in a magnetic field, neither the peak nor the low-energy side of the luminescence line yields an exact value for the single-particle band gap.

In wide-gap semiconductors many theoretical as well as experimental papers deal with the above-mentioned effects.⁶⁻¹² In IV-VI compounds like PbTe, PbSe, or $\text{Pb}_{1-x}\text{Eu}_x\text{Se}$, up to now the modifications of the band structure by exchange and correlation effects have been neglected using the argument of small effective masses and high dielectric constants of these materials.

The aim of the present paper is to demonstrate that even in IV-VI's many-particle effects have to be taken into account, and that band parameters deduced under the above-mentioned approximations from photoluminescence spectra are much less exact than data obtained by other methods like interband magnetotransmission, far-

infrared absorption, or coherent anti-Stokes Raman scattering.

In Sec. II a short review of band-structure calculations for diamagnetic and semimagnetic IV-VI compounds is given. Section III describes many-particle effects, with special emphasis on the case of a many-valley semiconductor with ellipsoidal surfaces of constant energy. The calculation of photoluminescence line shapes under consideration of spontaneous as well as stimulated emission is performed in Sec. IV. In Sec. V experimental results are reported and discussed. Section VI gives a short summary.

II. ENERGY-BAND STRUCTURE AND DENSITIES OF STATES OF (DILUTED MAGNETIC) LEAD CHALCOGENIDES

In order to model the band structure of lead chalcogenides and their semimagnetic alloys, several characteristics of these semiconductors have to be taken into account. The band extrema occur at the L points of the Brillouin zone, which results in nonspherical surfaces of constant energy and a many-valley structure of both valence and conduction bands. Furthermore the energy dispersion relations of these semiconductors are strongly nonparabolic due to the narrow direct energy gaps. However, in case of free-carrier concentrations smaller than about $5 \times 10^{19} \text{ cm}^{-3}$, the effects of nonparabolicity and the deviation of the surfaces of constant energy from

ellipsoids of revolution can be neglected approximately.^{13,14} In the single-particle picture the anisotropic energy dispersion relation of the conduction band is written as

$$\varepsilon^{\text{CB}}(\mathbf{k}) = \varepsilon^{\text{CB}}(0) + \frac{\hbar^2}{2m_0} \left[\frac{k_x^2 + k_y^2}{m_t^{\text{CB}}} + \frac{k_z^2}{m_l^{\text{CB}}} \right], \quad (1)$$

where m_0 denotes the free-electron mass, and m_t^{CB} and m_l^{CB} are the transverse and longitudinal effective masses of the conduction band (in units of m_0). From the corresponding volume $V_{F,e}(\varepsilon^{\text{CB}}(\mathbf{k}))$ of the Fermi ellipsoid, the density of states of the conduction band including spin degeneracy can be deduced:

$$g^{\text{CB}}(\varepsilon) = \nu \frac{2}{(2\pi)^3/V} \frac{\partial V_{F,e}(\varepsilon)}{\partial \varepsilon} \\ = \nu \frac{V}{2\pi^2} \left[\frac{2m_0 m_d^{\text{CB}}}{\hbar^2} \right]^{3/2} \sqrt{\varepsilon - \varepsilon^{\text{CB}}(0)}, \quad (2)$$

where V stands for the crystal volume, $\nu=4$ is the number of equivalent valleys, and $m_0 m_d^{\text{CB}} = m_0 ((m_t^{\text{CB}})^2 m_l^{\text{CB}})^{1/3}$ denotes the density-of-states effective mass of the conduction band. For the holes the formula analogous to Eq. (2) applies, the valence-band effective masses being defined as positive quantities for reasons quoted in Sec. III:

$$g^{\text{VB}}(\varepsilon) = \nu \frac{V}{2\pi^2} \left[\frac{2m_0 m_d^{\text{VB}}}{\hbar^2} \right]^{3/2} \sqrt{\varepsilon^{\text{VB}}(0) - \varepsilon}. \quad (3)$$

In the case of external magnetic fields the method for calculating the Landau levels of both the lowest conduction and the highest valence band of semimagnetic lead chalcogenides is reviewed by Bauer, Pascher, and Zawadzki.¹⁶ The treatment is based on the $\mathbf{k} \cdot \mathbf{p}$ model of Mitchell and Wallis.¹⁶ In Ref. 15 the Hamiltonians, which have to be diagonalized in order to obtain the Landau-level energies

$$g_B^{\text{CB}}(\varepsilon) = \frac{eBV}{\sqrt{2}\pi^2 \hbar^2} \sum_{\Phi} Z(\Phi) \sqrt{m_0 m_B^{\text{CB}}(\Phi)} \sum_{n_L^{\text{CB}}} \frac{1}{2} \sum_{m_s^{\text{CB}}} \Gamma_{\tau_{g,e}} \left[\frac{1}{\sqrt{\varepsilon - \varepsilon_L^{\text{CB}}(\Phi, n_L^{\text{CB}}, m_s^{\text{CB}})}} \right], \quad (6)$$

$$g_B^{\text{VB}}(\varepsilon) = \frac{eBV}{\sqrt{2}\pi^2 \hbar^2} \sum_{\Phi} Z(\Phi) \sqrt{m_0 m_B^{\text{VB}}(\Phi)} \sum_{n_L^{\text{VB}}} \frac{1}{2} \sum_{m_s^{\text{VB}}} \Gamma_{\tau_{g,h}} \left[\frac{1}{\sqrt{\varepsilon_L^{\text{VB}}(\Phi, n_L^{\text{VB}}, m_s^{\text{VB}}) - \varepsilon}} \right], \quad (7)$$

where $\Gamma_{\tau_g}()$ denotes the usual Lorentzian broadening function:

$$\Gamma_{\tau_{g,e}} \left[\frac{1}{\sqrt{\varepsilon - \varepsilon_L^{\text{CB}}}} \right] \\ = \left[\frac{\varepsilon - \varepsilon_L^{\text{CB}} + \sqrt{(\varepsilon - \varepsilon_L^{\text{CB}})^2 + \hbar^2/\tau_{g,e}^2}}{2[(\varepsilon - \varepsilon_L^{\text{CB}})^2 + \hbar^2/\tau_{g,e}^2]} \right]^{1/2}. \quad (8)$$

Assuming $\tau_{g,e} = \tau_{g,h} \equiv \tau_g$, the average collision time τ_g is

TABLE I. Angle Φ between the main ellipsoidal axis and magnetic-field direction \mathbf{B} , and the number of ellipsoids $Z(\Phi)$ in Faraday and Voigt geometries, respectively (surface normal of the epitaxial films grown on BaF_2 is parallel to the [111] direction).

Geometry	Angle Φ	Number $Z(\Phi)$
Faraday	0°	1
$\mathbf{B} \parallel [111]$	70.53°	3
Voigt	35.26°	2
$\mathbf{B} \parallel [1\bar{1}0]$	90.00°	2

$\varepsilon_L^{\text{CB}}(\Phi, n_L^{\text{CB}}, m_s^{\text{CB}})$ and $\varepsilon_L^{\text{VB}}(\Phi, n_L^{\text{VB}}, m_s^{\text{VB}})$, are given explicitly. In the parabolic approximation the corresponding energy dispersion relations are

$$\varepsilon^{\text{CB}}(\Phi, k_B^{\text{CB}}, n_L^{\text{CB}}, m_s^{\text{CB}}) \\ = \varepsilon^{\text{CB}}(0) + \varepsilon_L^{\text{CB}}(\Phi, n_L^{\text{CB}}, m_s^{\text{CB}}) + \frac{\hbar^2 (k_B^{\text{CB}})^2}{2m_0 m_B^{\text{CB}}(\Phi)}, \quad (4)$$

$$\varepsilon^{\text{VB}}(\Phi, k_B^{\text{VB}}, n_L^{\text{VB}}, m_s^{\text{VB}}) \\ = \varepsilon^{\text{VB}}(0) + \varepsilon_L^{\text{VB}}(\Phi, n_L^{\text{VB}}, m_s^{\text{VB}}) - \frac{\hbar^2 (k_B^{\text{VB}})^2}{2m_0 m_B^{\text{VB}}(\Phi)}, \quad (5)$$

where $n_L^{\text{CB/VB}}$ and $m_s^{\text{CB/VB}}$ denote Landau quantum numbers and magnetic spin quantum numbers, $k_B^{\text{CB/VB}}$ are the components of the electrons and holes' quasimomentum in the direction of \mathbf{B} , and $m_B^{\text{CB/VB}}(\Phi)$ are the effective masses (in units of m_0) of conduction and valence bands along the magnetic field. Φ denotes the angle between the magnetic-field direction and the respective valley axis; see Table I.

The densities of states, corresponding to Eqs. (4) and (5), are

connected to the Dingle temperature in the following way:¹⁷

$$T_D = \frac{\hbar}{\pi k_B \tau_g}, \quad (9)$$

where k_B is Boltzmann's constant.

Taking τ_g to be independent of the energy ε , approximation (8) causes the carrier densities to tend to infinity, due to the long tail of the densities of states for energies below the bottom of the lowest magnetic subband.¹⁸ Therefore the cutoff energies

$$\varepsilon_{\text{cutoff}}^{\text{CB}} = \varepsilon^{\text{CB}}(0) + \min\{\varepsilon_L^{\text{CB}}(\Phi, n_L^{\text{CB}}, m_s^{\text{CB}})\} - 2\hbar/\tau_g, \quad (10)$$

$$\varepsilon_{\text{cutoff}}^{\text{VB}} = \varepsilon^{\text{VB}}(0) + \max\{\varepsilon_L^{\text{VB}}(\Phi, n_L^{\text{VB}}, m_s^{\text{VB}})\} + 2\hbar/\tau_g \quad (11)$$

according to Götze and Hajdu¹⁹ are used in order to calculate the electron and hole densities which enter the exchange and correlation energy terms.

III. MANY-PARTICLE EFFECTS

The high excitation intensities often used in photoluminescence experiments result in concentrations of photoexcited carriers of the order 10^{16} to 10^{18} cm^{-3} . Furthermore lead chalcogenides are characterized by hole or electron concentrations of the order 10^{17} cm^{-3} due to defects. Therefore many-particle effects have to be taken into account for a theoretical description of the experimentally observed spectral line shapes and line positions of the recombination radiation. The main effect of many-particle interactions on photoluminescence line shapes calculated in the single-particle picture is the scaling with an enhancement factor because of matrix element renormalizations.^{8,20} The wavelength dependence of this factor, however, can be neglected over the spectral range of a photoluminescence line. Furthermore the small renormalizations of effective masses and mass anisotropies²¹ are not taken into account in the following treatment. The main effect of many-particle interactions is the reduction of the single-particle band gap $\varepsilon_g = \varepsilon^{\text{CB}}(0) - \varepsilon^{\text{VB}}(0)$ due to exchange and correlation energy terms, which results in a redshift of the position of a photoluminescence line.

Without external magnetic field, the Hartree-Fock energy $E_{\text{HF},e} = E_{\text{kin},e} + E_{\text{exch},ee}$ of interacting electrons in the conduction band of a many-valley semiconductor with ellipsoids of revolution as surfaces of constant energy can be obtained exactly. The calculation for $T=0$ has been carried out by Combescot and Nozieres.²² In the case of quadratic dispersion laws [see, e.g., Eq. (1)], the averaged kinetic energy per particle $E_{\text{kin},e}/N$ (N being the number of electrons) does not depend on the shape of the Fermi surface but only on the appropriate quasi-Fermi level of the conduction band $\varepsilon_F^{\text{CB}} = \hbar^2 k_{F,e}^2 / 2m_0 m_d^{\text{CB}}$:

$$\begin{aligned} \frac{E_{\text{kin},e}}{N} &= \frac{1}{n} 2 \int_{V_F(\gamma_e)} \frac{d\mathbf{k}}{(2\pi)^3} \frac{\hbar^2 \mathbf{k}^2}{2m_0 m_d^{\text{CB}}} \\ &= \frac{3}{5} \varepsilon_F^{\text{CB}} = \frac{3}{10} \frac{\hbar^2 (3\pi^2 n / \nu)^{2/3}}{m_0 m_d^{\text{CB}}}, \end{aligned} \quad (12)$$

where $n = N/V$ denotes the density of free electrons.

The averaged exchange energy per electron can be obtained from the following integration over the ellipsoidal Fermi volume $V_{F,e}(\gamma_e)$, with $\gamma_e = m_i^{\text{CB}} / m_l^{\text{CB}}$:

$$\begin{aligned} \frac{E_{\text{exch},ee}}{N} &= -\frac{1}{n} \frac{1}{4\pi\varepsilon_r\varepsilon_0} \int \int_{V_{F,e}(\gamma_e)} \frac{d\mathbf{k} d\mathbf{k}'}{(2\pi)^6} \frac{4\pi e^2}{|\mathbf{k} - \mathbf{k}'|^2} \\ &= -\frac{e^2}{4\pi\varepsilon_r\varepsilon_0} \frac{3}{4\pi} k_{F,e} \varphi(\gamma_e), \end{aligned} \quad (13)$$

where $\varphi(\gamma_e)$ accounts for the anisotropy:

$$\varphi(\gamma_e) = \gamma_e^{1/6} \left[\frac{\arcsin \sqrt{1-\gamma_e}}{\sqrt{1-\gamma_e}} \theta(1-\gamma_e) + \frac{\arcsin \sqrt{1-1/\gamma_e}}{\sqrt{\gamma_e-1}} \theta(\gamma_e-1) \right]. \quad (14)$$

In usual numerical units, the Hartree-Fock energy per particle is then given by

$$\frac{E_{\text{HF},e}}{N} = \left[\frac{2.2099}{r_{s,e}^2 \nu^{2/3}} - \frac{0.9163}{r_{s,e} \nu^{1/3}} \varphi(\gamma_e) \right] E_{R,\text{eff}}^{\text{CB}}. \quad (15)$$

$E_{R,\text{eff}}^{\text{CB}} = E_R m_d^{\text{CB}} / \varepsilon_r^2$ denotes the effective rydberg and $r_{s,e} = \sqrt[3]{3/(4\pi n)} / (a_0 \varepsilon_r / m_d^{\text{CB}})$ is the average interparticle spacing in units of the effective Bohr radius.

Because of the direct energy gaps of IV-VI compounds, the lifetime of the photoexcited electrons and holes is comparatively small and therefore the effective temperature T_{eff} of the carrier subsystem differs substantially from the lattice temperature T_L of the sample. Thus the limit $T=0$ K is not a good approximation in that case, even with lattice temperatures T_L below 2 K. Consequently, the electron density n and the integrals occurring in the kinetic [Eq. (12)] and exchange energies [Eq. (13)] have to be calculated numerically. Thereby the electronic density of states of the conduction band $g_e^{\text{CB}}(\varepsilon)$ and the Fermi distribution function of the electrons in the conduction band $f_e^{\text{CB}}(\varepsilon, T_{\text{eff}})$, including the quasi-Fermi Level $\mu^{\text{CB}}(T_{\text{eff}})$ for $T = T_{\text{eff}}$, have to be used.

The averaged exchange energy per particle $E_{\text{exch},ee}/N$ only includes the Coulomb interaction between electrons in the same spin state. Further interaction energy terms of a many-particle system, going beyond the Hartree-Fock approximation, are defined as the correlation energy.²³ The averaged correlation energy per electron in the conduction band of an anisotropic many-valley semiconductor can easily be estimated over the whole range of the density parameter $r_{s,e}$ using Wigner's numerical interpolation formula²⁴

$$\frac{E_{\text{corr},ee}}{N} = -\frac{0.88}{r_{s,e} \nu^{1/3} + 7.80} E_{R,\text{eff}}^{\text{CB}}. \quad (16)$$

Furthermore, in the high-density range $r_{s,e} \ll 1$, the following simple generalization of the expression given by Gell-Mann and Brueckner,²³ is a good approximation:

$$\frac{E_{\text{corr},ee}}{N} = [0.0622 \ln(r_{s,e} \nu^{1/3}) - 0.096] E_{R,\text{eff}}^{\text{CB}}. \quad (17)$$

Just as in Eq. (16), the temperature dependence is included implicitly by $n(T_{\text{eff}})$. Compared to the exchange energy term [Eq. (13)], the correlation energy calculated by either of these formulas is small in the density range of interest.

For the interacting holes in the valence band, the relevant energy terms can be calculated in analogy to Eqs. (12)–(17).

In $\text{Pb}_{1-x}\text{Eu}_x\text{Se}$ there is a considerable number of free holes due to doping. They contribute to the exchange

and correlation energy of the valence band. As a consequence, the Hartree-Fock energy of $\text{Pb}_{1-x}\text{Eu}_x\text{Se}$ does not show a pronounced minimum in the whole range of the electron hole pair density (see Fig. 1). Thus a homogeneous electron-hole plasma without any phase separation is expected to be observable in photoluminescence experiments at all excitation intensities.

As mentioned above, the exchange and correlation energy terms result in a renormalization of the single-particle band gap represented by the carrier-density-dependent electron-hole-plasma shift $\Delta\epsilon_{\text{EHP}}(\epsilon_r)$. Neglecting electron-hole correlations, the EHP shift in the case of a spatially homogeneous electron-hole plasma is given by⁶

$$\Delta\epsilon_{\text{EHP}}(\epsilon_r) = \frac{E_{\text{exch,ee}}(\epsilon_r) + E_{\text{corr,ee}}(\epsilon_r)}{N} + \frac{E_{\text{exch,hh}}(\epsilon_r) + E_{\text{corr,hh}}(\epsilon_r)}{P}. \quad (18)$$

In order to obtain symmetry in signs for the exchange and correlation energy terms of both electrons and holes, the valence-band effective masses have been defined to be positive quantities, as mentioned in Sec. II.

In the case of experimentally caused spatial inhomogeneities of the carrier plasma in a direct-gap semiconductor, which are not to be mixed up with the phase separation of the plasma observed in indirect-gap semiconductors (\rightarrow electron-hole droplets EHD), the following expression^{8,12} has to be added to the sum of exchange and correlation energy terms on the right-hand side of Eq. (18):

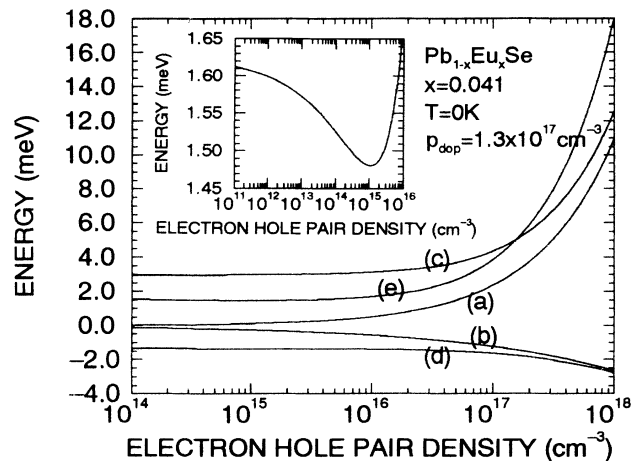


FIG. 1. Different many-particle energy terms as a function of electron-hole pair density, calculated using the high-frequency dielectric constant $\epsilon_{r,\infty}$; background doping $p = 1.3 \times 10^{17} \text{ cm}^{-3}$. Curve a: Averaged kinetic energy per electron. Curve b: Averaged exchange energy per electron. Curve c: Averaged kinetic energy per hole. Curve d: Averaged exchange energy per hole. Curve e: Sum of Hartree-Fock energies of conduction and valence bands [sum of contributions (a)–(d)]. Inset: curve e with changed scales.

$$n \frac{\partial}{\partial n} \left[\frac{E_{\text{exch,ee}} + E_{\text{corr,ee}}}{N} \right] + p \frac{\partial}{\partial p} \left[\frac{E_{\text{exch,hh}} + E_{\text{corr,hh}}}{P} \right]. \quad (19)$$

For strongly polar semiconductors like the lead salts, the electron (hole)–LO-phonon coupling has to be considered in addition to the exchange and correlation energy terms in order to calculate the ground-state energy of an interacting electron-hole plasma. The corresponding polaron shift⁷ $\Delta\epsilon_{P,e} + \Delta\epsilon_{P,h}$ also results in a reduction of the band gap with respect to the single-particle picture:

$$\Delta\epsilon_{P,e} + \Delta\epsilon_{P,h} = -\alpha_e \varphi(\gamma_e) \omega_{\text{LO}} - \alpha_h \varphi(\gamma_h) \omega_{\text{LO}}. \quad (20)$$

ω_{LO} denotes the frequency of the longitudinal-optical phonon, and α_e and α_h are the polar coupling constants for electrons and holes, respectively:

$$\alpha_{e/h} = \frac{e^2}{4\pi\epsilon_0} \left[\frac{1}{\epsilon_{r,\infty}} - \frac{1}{\epsilon_{r,0}} \right] \sqrt{m_0 m_d^{\text{CB/VB}} / 2\hbar\omega_{\text{LO}}}. \quad (21)$$

The relative contributions of the EHP shift and of the polaron shift to the total self-energy, which has to be added to the energy dispersion relations valid in the single-particle picture, depends on the carrier densities as well as whether the static or the high-frequency dielectric constant enters the exchange and correlation energy terms.²⁵ In the limit of very small electron and hole densities ($r_{s,e} \gg 1, r_{s,h} \gg 1$, which means plasma frequency ω_p is much smaller than LO-phonon frequency ω_{LO}); the self-energy shift is approximately given by the sum of the EHP shift (calculated with the static limit of the background dielectric constant) and of the polaron shift ($\epsilon_{r,0}$ approximation^{7,25}):

$$\lim_{n,p \rightarrow 0} (\Delta\epsilon_g) = \Delta\epsilon_{\text{EHP}}(\epsilon_{r,0}) + \Delta\epsilon_{P,e} + \Delta\epsilon_{P,h}. \quad (22)$$

In the limit of very high carrier densities ($r_{s,e} \ll 1, r_{s,h} \ll 1$) the EHP shift dominates the polaron shift ($\omega_{\text{LO}} \ll \omega_p$) and the former can be calculated by using the high-frequency dielectric constant ($\epsilon_{r,\infty}$ approximation^{7,25}):

$$\lim_{n,p \rightarrow \infty} (\Delta\epsilon_g) = \Delta\epsilon_{\text{EHP}}(\epsilon_{r,\infty}). \quad (23)$$

In contrast to the $\epsilon_{r,0}$ approximation, the $\epsilon_{r,\infty}$ approximation results in a pronounced increase of the energy-gap renormalization with plasma density, as shown in Fig. 2.

In the intermediate density range, the calculation of the ground-state energy of an interacting electron-hole plasma in polar semiconductors, and therefore the calculation of the self-energy terms, is much more difficult; e.g., see Refs. 7, 25, 26, and 27.

Whereas, in the above case $B=0$, the Hartree-Fock energy can be obtained exactly even under consideration of the band-structure characteristics of the lead chalcogenides, in the case of external magnetic fields a quantitative treatment of many-body effects to our knowledge is only possible, if one assumes an *idealized* band structure. Corresponding calculations in the limit of high magnetic fields and in the limit of high densities of an equilibrium

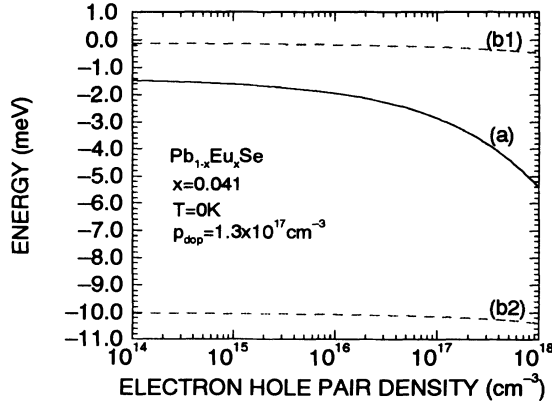


FIG. 2. Comparison of band-gap renormalization as a function of electron-hole pair density; background doping $p = 1.3 \times 10^{17} \text{ cm}^{-3}$. (a) $\epsilon_{r,\infty}$ approximation. (b2) $\epsilon_{r,0}$ approximation (including polaron shift). (b1) Sum of exchange and correlation energy terms calculated using the static dielectric constant $\epsilon_{r,0}$.

electron-hole plasma result in power-law dependencies of the exchange energy on the magnetic-field strength: $|E_{\text{exch},ee}/N + E_{\text{exch},hh}/P| \propto B^{1/3}$ and $|E_{\text{exch},ee}/N + E_{\text{exch},hh}/P| \propto B^{2/7}$, respectively.^{28,29}

$$dr_{\text{stim}}(\hbar\omega) = -\frac{n_r^2(\hbar\omega)^2}{\pi^2 c^2 \hbar^3} \alpha(\hbar\omega), \quad (25)$$

$$dr_{\text{spont}}(\hbar\omega) = dr_{\text{stim}}(\hbar\omega) \left\{ 1 - \exp \left[\frac{\hbar\omega - [\mu^{\text{CB}}(T_{\text{eff}}) - \mu^{\text{VB}}(T_{\text{eff}})]}{k_B T_{\text{eff}}} \right] \right\}^{-1}, \quad (26)$$

where n_r denotes the index of refraction, and c is the vacuum speed of light.

The absorption constant $\alpha(\hbar\omega)$ for $B=0$ is given in the spherical and parabolic approximation as

$$\alpha(\hbar\omega) \propto \frac{(m_d^{\text{red}})^{3/2}}{n_r \hbar\omega} |P|^2 \sqrt{\hbar\omega - (\epsilon_g + \Delta\epsilon_g)} \times [f_e^{\text{VB}}(\epsilon_a(k)) - f_e^{\text{CB}}(\epsilon_b(k))], \quad (27)$$

$m_0 m_d^{\text{red}}$ standing for the reduced density-of-states effective mass. The matrix element P connecting the states $|a\rangle$ of the valence and $|b\rangle$ of the conduction band is considered to be k independent. The difference $f_e^{\text{VB}} - f_e^{\text{CB}}$ of the Fermi distribution functions takes into account $T_{\text{eff}} \neq 0$ (\rightarrow Burstein-Moss shift) and reflects the inclusion of stimulated downward transitions: $f_e^{\text{VB}} - f_e^{\text{CB}} = (1 - f_e^{\text{CB}}) f_e^{\text{VB}} - f_e^{\text{CB}} (1 - f_e^{\text{VB}})$. Within the framework of the above-mentioned approximations, the energies $\epsilon_a(k)$ and $\epsilon_b(k)$ of levels $|a\rangle$ and $|b\rangle$ can be obtained as (taking zero of energy at the renormalized valence-band edge)

$$\epsilon_a(k) = \frac{m_d^{\text{red}}}{m_d^{\text{VB}}} (\epsilon_g + \Delta\epsilon_g - \hbar\omega), \quad (28)$$

IV. PHOTOLUMINESCENCE LINE SHAPES OF IV-VI COMPOUNDS

Due to very high dielectric constants and to the small effective masses of both electrons and holes, contributions of excitons and shallow impurities to the photoluminescence spectra of (semimagnetic) lead chalcogenides are not expected, particularly for relatively high carrier temperatures and densities.

In the case of an ideally perfect crystal, only k -conserving direct interband transitions are allowed. If it is possible to transfer momentum to crystal imperfections under negligible change in energy, additional band-to-band transitions can take place under violation of that conservation law.

For k -conserving interband transitions, the calculation of the microscopic spontaneous emission rate $dr_{\text{spont}}(\hbar\omega)$ and of the microscopic net stimulated emission rate $dr_{\text{stim}}(\hbar\omega)$ starts from the absorption constant $\alpha(\hbar\omega)$, which is dependent on the quantum energy $\hbar\omega$ of the emitted recombination radiation:

$$\alpha(\hbar\omega) \Rightarrow dr_{\text{stim}}(\hbar\omega) \Rightarrow dr_{\text{spont}}(\hbar\omega). \quad (24)$$

The relationships between the quantities in Eq. (24) are given, according to Lasher and Stern,³⁰ by

$$\epsilon_b(k) = \frac{m_d^{\text{red}}}{m_d^{\text{VB}}} [\epsilon_g + \Delta\epsilon_g + (m_d^{\text{VB}}/m_d^{\text{CB}}) \hbar\omega], \quad (29)$$

with $\epsilon_b(k) - \epsilon_a(k) = \hbar\omega$. It should be noted that $dr_{\text{stim}}(\hbar\omega)$ and therefore $dr_{\text{spont}}(\hbar\omega)$ is also compatible with the use of a Slater determinant for the wave function of the many-particle system under consideration; see Ref. 31.

Beyond the spherical approximation, a more sophisticated treatment of the anisotropy of the surfaces of constant energy,³² taking into account ellipsoids of revolution when calculating the absorption constant, results in the additional energy-dependent factor $(\hbar\omega + \epsilon_g + \Delta\epsilon_g)^{3/2}$. Its variation with wavelength, however, can be neglected over the range of a photoluminescence line, and therefore the consideration of anisotropy beyond the use of the density-of-state effective masses in Eqs. (27)–(29) does not affect the spectral line shape. The absorption constant of an anisotropic many-valley semiconductor exposed to an external magnetic field can be obtained as an extension of the expression given by Roth, Lax, and Zwerdling,³³ taking into account $T_{\text{eff}} \neq 0$:

$$\alpha_B(\hbar\omega) \propto \sum_{\Phi} \frac{B}{n_r \hbar\omega} Z(\Phi) \sqrt{m_B^{\text{red}}(\Phi)} |P_B(\Phi)|^2 \sum_{\text{allowed transitions}} \Gamma_{\tau_\alpha} \left[\frac{1}{\sqrt{\hbar\omega - \hbar\Omega}} \right] [f_e^{\text{VB}}(\epsilon_a) - f_e^{\text{CB}}(\epsilon_b)]. \quad (30)$$

The degeneracy of the different parts of the Fermi surface is lifted for $B \neq 0$ (see Table I), and therefore the effective masses $m_B^{\text{CB/VB}}(\Phi)$ along the magnetic field as well as the transition matrix element $P_B(\Phi)$, depend on Φ :^{33,15}

$$m_B^{\text{CB/VB}}(\Phi) = m_t^{\text{CB/VB}} \cos^2(\Phi) + m_l^{\text{CB/VB}} \sin^2(\Phi), \quad (31)$$

$$|P_B(\Phi)|^2 = P_\perp^2 \sqrt{\cos^2\Phi + (P_\perp/P_\parallel)^{-2} \sin^2\Phi}. \quad (32)$$

On the right-hand side of Eq. (30) the summation over all pairs of Landau levels, connected with one another by the interband selection rules³⁴ given in Table II, occurs.

The corresponding energy differences, appearing in the argument of the Lorentzian broadening function Γ_{τ_α} (with $\tau_\alpha = \tau_g/2$) include the many-body renormalization of the band gap:

$$\hbar\Omega = \epsilon_g + \Delta\epsilon_g + \bar{\epsilon}_L^{\text{CB}} - \bar{\epsilon}_L^{\text{VB}}, \quad (33)$$

where $\bar{\epsilon}_L^{\text{CB}}$ and $\bar{\epsilon}_L^{\text{VB}}$ denote the energies of the Landau levels relative to their respective renormalized band edges. The energies $\epsilon_a(k_B)$ and $\epsilon_b(k_B)$ of levels $|a\rangle$ and $|b\rangle$ can be calculated in the parabolic approximation concerning k_B [see Eqs. (4) and (5)] as follows:

$$\epsilon_a(k_B) = \frac{m_B^{\text{red}}}{m_B^{\text{CB}}} \bar{\epsilon}_L^{\text{VB}} + \frac{m_B^{\text{red}}}{m_B^{\text{VB}}} (\epsilon_g + \Delta\epsilon_g + \bar{\epsilon}_L^{\text{CB}} - \hbar\omega), \quad (34)$$

$$\epsilon_b(k_B) = \frac{m_B^{\text{red}}}{m_B^{\text{VB}}} (\epsilon_g + \Delta\epsilon_g + \bar{\epsilon}_L^{\text{CB}}) + \frac{m_B^{\text{red}}}{m_B^{\text{CB}}} (\bar{\epsilon}_L^{\text{VB}} + \hbar\omega), \quad (35)$$

in analogy to Eqs. (28) and (29) in the case of vanishing magnetic field.

The combined density of states is the fundamental quantity for the theoretical description of \mathbf{k} -conserving interband transitions. The individual densities of states of both conduction and valence bands become important in the case of band-to-band transitions without conserving the electrons quasimomentum. When calculating the microscopic emission rates in the latter case, all occupied electron and hole states have to be integrated, fulfilling energy conservation:³⁰

$$dr_{\text{spon}}(\hbar\omega) \propto \hbar\omega \int g^{\text{CB}}(\epsilon') g^{\text{VB}}(\epsilon' - \hbar\omega) f_e^{\text{CB}}(\epsilon') \times [1 - f_e^{\text{VB}}(\epsilon' - \hbar\omega)] d\epsilon', \quad (36)$$

TABLE II. Interband selection rules in the case of an externally applied magnetic field.

Geometry	Polarization of light	Selection rules
Faraday $\mathbf{K} \parallel \mathbf{B} \parallel [111]$	σ^+ (right circular)	$\Delta n_L = 0; \Delta m_s = -1$
	σ^- (left circular)	$\Delta n_L = 0; \Delta m_s = +1$
Voigt $\mathbf{K} \perp \mathbf{B}; \mathbf{B} \parallel [1\bar{1}0]$	$\mathbf{E} \parallel \mathbf{B}$ (linear)	$\Delta n_L = 0; \Delta m_s = 0$
	$\mathbf{E} \perp \mathbf{B}$ (linear)	$\Delta n_L = 0; \Delta m_s = \pm 1$

$$dr_{\text{stim}}(\hbar\omega) \propto \hbar\omega \int g^{\text{CB}}(\epsilon') g^{\text{VB}}(\epsilon' - \hbar\omega) \times [f_e^{\text{CB}}(\epsilon') - f_e^{\text{VB}}(\epsilon' - \hbar\omega)] d\epsilon'. \quad (37)$$

Again, the interband matrix elements and the index of refraction are assumed to be energy independent over the wavelength range of interest. For $B=0$ as well as $B \neq 0$ the densities of states, which are to be inserted into Eqs. (36) and (37), are given according to Eqs. (2) and (3) and (4) and (5), respectively. Note, however, that interactions between carriers in different valleys usually are not taken into account, and therefore in the case $B \neq 0$ the summation over Φ in the densities of states (4) and (5) is dropped and the microscopic rates according to Eqs. (36) and (37) have to be calculated separately for each kind of valley.

With the help of the microscopic emission functions $dr_{\text{spon}}(\hbar\omega)$ and $dr_{\text{stim}}(\hbar\omega)$ given above, the macroscopic emission rates $I_{\text{spon}}(\hbar\omega)$ and $I_{\text{stim}}(\hbar\omega)$, i.e., the photoluminescence line shapes, can be obtained. Spontaneous emission is a linear optical process, and therefore the corresponding spectral line shapes observed in experiment are directly proportional to the microscopic emission rates:

$$I_{\text{spon}}(\hbar\omega) \propto dr_{\text{spon}}(\hbar\omega). \quad (38)$$

In contrast, when stimulated emission is the dominating recombination process, e.g., at higher excitation intensities I_{exc} , the photoluminescence line shapes caused by super-radiance can be calculated within the model of a one-dimensional optical amplifier:³⁵

$$I_{\text{stim}}(\hbar\omega) \propto \frac{dr_{\text{spon}}(\hbar\omega)}{dr_{\text{stim}}(\hbar\omega)} \{ \exp[g(I_{\text{exc}}, \hbar\omega) L_{\text{eff}}(\hbar\omega)] - 1 \}, \quad (39)$$

where saturation effects have been neglected. $L_{\text{eff}}(\hbar\omega)$ denotes an effective length over which the amplification of the spontaneous emission takes place, and $g(I_{\text{exc}}, \hbar\omega)$ is the net optical gain per unit length, which is proportional to the microscopic stimulated net emission rate $dr_{\text{stim}}(\hbar\omega)$:

$$g(I_{\text{exc}}, \hbar\omega) = C(I_{\text{exc}}) dr_{\text{stim}}(\hbar\omega). \quad (40)$$

$C(I_{\text{exc}})$ goes to zero as I_{exc} goes to zero, and therefore in this limit the spectral intensity distribution of the super-radiance $I_{\text{stim}}(\hbar\omega)$ reduces to $I_{\text{spon}}(\hbar\omega)$.

The theoretical photoluminescence line shapes corresponding to the cases of purely spontaneous and purely stimulated emission are shown in Fig. 3 for $B=0$. Using the same set of plasma parameters, interband transitions taking place under violation of the \mathbf{k} -selection rule (broken lines in Fig. 3) result in a shift of the recombination radiation maximum toward shorter wavelengths with respect to luminescence lines arising from \mathbf{k} -conserving band-to-band transitions (full lines in Fig. 3).

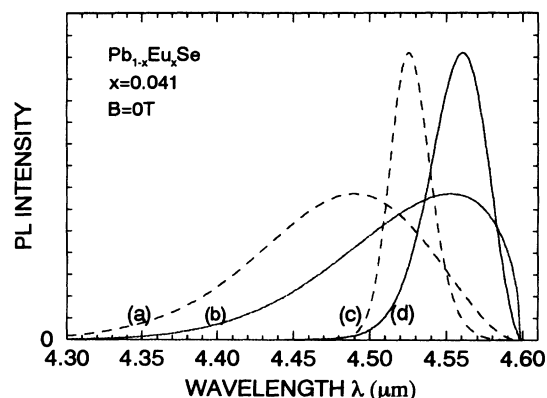


FIG. 3. Calculated photoluminescence line shapes $T_{\text{eff}}=20$ K, $\mu^{\text{CB}}(20\text{ K})=0.75$ meV, $\mu^{\text{VB}}(20\text{ K})=-5.50$ meV, $\epsilon_g=274.00$ meV, $\epsilon_g+\Delta\epsilon_g=269.68$ meV, and $gL_{\text{eff}}=5$. (a) Spontaneous emission without \mathbf{k} conservation. (b) Spontaneous emission with \mathbf{k} conservation. (c) Stimulated emission without \mathbf{k} conservation. (d) Stimulated emission with \mathbf{k} conservation. Note that the theoretical curves shown in this figure have been plotted with arbitrarily chosen scaling factors.

For $B \neq 0$, theoretical photoluminescence line shapes of spontaneous emission with conservation of the component k_B of the quasimomentum along the magnetic field yield sharp extrema in the macroscopic emission rate, corresponding to individual Landau levels. Sharp peaks disappear with the increasing importance of carrier-carrier and carrier-defect scattering [see Fig. 4(a)]. For interband transitions violating the k_B -selection rule, these extrema are smeared out at even smaller values of τ_α . However, with the increasing importance of stimulated emission, the spectra (macroscopic emission rates) are expected to show sharper peaks again [see Fig. 4(b)], thereby amplifying the interband transition between Landau levels with the highest microscopic emission rate dominantly [see Eq. (39)].

V. EXPERIMENTAL RESULTS AND DISCUSSION

A. Band-gap renormalization without magnetic field

In order to study the dependence of the band-gap renormalization on the carrier densities quantitatively, photoluminescence measurements were performed without external magnetic field at $T_L=1.7$ K on p -type $\text{Pb}_{1-x}\text{Eu}_x\text{Se}$ ($x=0.041$, epitaxial film on BaF_2 grown by molecular-beam epitaxy^{36,37}) at different excitation intensities. The spectra shown in Fig. 5 were taken in back-scattering geometry with the sample tilted by about 30° from the normal incidence position. Thus a change of photoluminescence line shapes and line positions due to resonator effects can be avoided. Photoluminescence was excited by the radiation of a Q -switched Nd:YAG (yttrium aluminum garnet) laser, its intensity attenuated enough to avoid damage of the sample surface ($I_0 \cong 1.3$ GW/m² being the maximum pump intensity used in our experiments). The fits (broken lines in Fig. 5) are calcu-

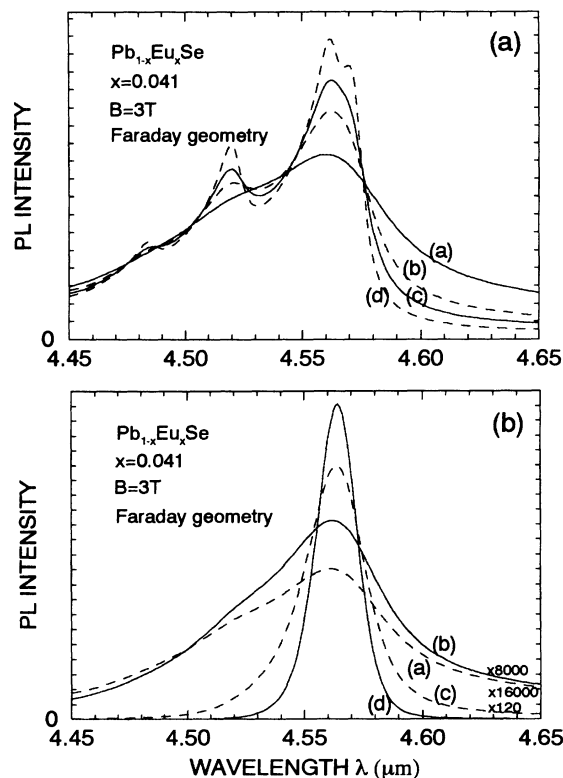


FIG. 4. (a) Calculated magnetophotoluminescence line shapes ($B=3\text{ T}$) with k_B conservation, parameters as in Fig. 3. Curve a: $\tau_\alpha=0.5 \times 10^{-12}$ s. Curve b: $\tau_\alpha=1.0 \times 10^{-12}$ s. Curve c: $\tau_\alpha=1.5 \times 10^{-12}$ s. Curve d: $\tau_\alpha=2.5 \times 10^{-12}$ s. (b) Calculated magnetophotoluminescence line shapes ($B=3\text{ T}$) with different amounts of stimulated emission, parameters as in Fig. 4(a), curve a. Curve a: $gL_{\text{eff}}=0.5$. Curve b: $gL_{\text{eff}}=1.0$. Curve c: $gL_{\text{eff}}=5.0$. Curve d: $gL_{\text{eff}}=10.0$.

lated using the theory of \mathbf{k} -conserving interband transitions. The following quantities were independently varied when making line-shape fits to experimental spectra: T_{eff} , $\mu^{\text{CB}}(T_{\text{eff}})$, $\mu^{\text{VB}}(T_{\text{eff}})$, ϵ_g , gL_{eff} and, for $B \neq 0$, τ_α . In order to obtain good quantitative agreement between experiment and theory, it has to be assumed that the spectra are dominated by stimulated emission even at the lowest excitation level with a background due to spontaneous emission, the relative strength of which increases with decreasing excitation intensity. The theoretical line shapes were obtained neglecting any additional tails (Urbach tail, line broadening because of spatial energy gap fluctuations, etc.) in the combined density of states. This simplification does not affect the accuracy of a determination of the parameters characteristic of the electron hole plasma, especially in the case of the spectra dominated by stimulated emission. This is explained by the exponential amplification of the microscopic emission rate in the case of super-radiance [see Eq. (39)].

The corresponding net optical gain, resulting from the line-shape analysis, taking L_{eff} to be the thickness of the sample, is shown as a function of the normalized excitation intensity I_{exc}/I_0 in Fig. 6. For pump intensities not far below the threshold for sample damage the gain is ap-

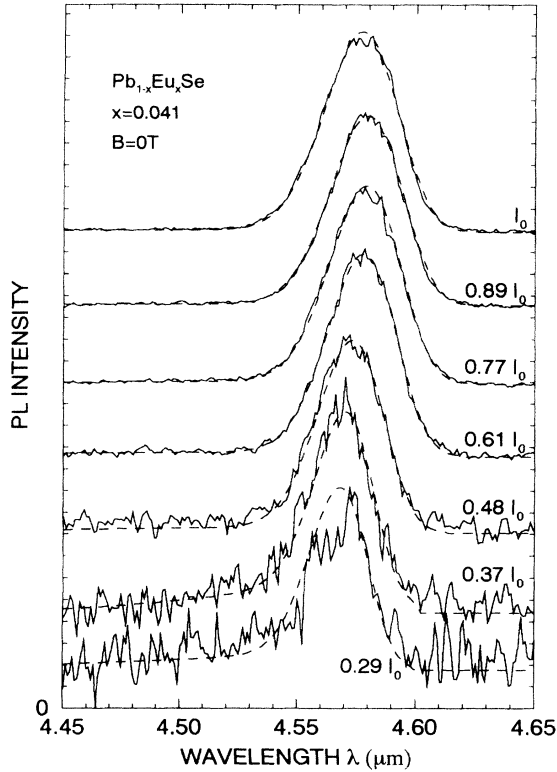


FIG. 5. Comparison of photoluminescence spectra with different excitation intensities. ($I_0=1.3 \text{ GW/m}^2$, backscattering geometry). Broken lines: calculated line shapes (see text; parameters as plotted in Figs. 6–8).

proximately $g_{\text{max}} \cong 1.3 \times 10^4 \text{ cm}^{-1}$, which is the same order of magnitude as observed in direct wide-gap semiconductors.³⁸

For $B=0$ the exchange energy terms in the Hartree-Fock energy can be obtained exactly, even in the case of the rather complicated energy-band-structure of the lead salts. The renormalization of the band gap due to many particle interactions of both electrons and holes was taken into account according to Eqs. (17), (18), (19), and (23). The experimentally observed dependence of the band-gap shift on the carrier densities (obtained from the effective carrier temperature and the quasi-Fermi levels fitted to the spectra) is in agreement with the $\epsilon_{r,\infty}$ approximation. In contrast, despite yielding a larger total self-energy shift, the $\epsilon_{r,0}$ approximation results in exchange and correlation energy terms being too weakly dependent on the electron-hole-plasma density and, therefore, in the framework of this approximation one cannot explain the change in the observed spectra resulting from a variation of the excitation intensity.

Note that the reduced band gap $\epsilon_g + \Delta\epsilon_g$ and the quasi-Fermi levels $\mu^{\text{CB}}(T_{\text{eff}})$ and $\mu^{\text{VB}}(T_{\text{eff}})$ cannot be chosen as independent fit parameters, because the band-gap renormalization $\Delta\epsilon_g$ and the quasi-Fermi levels are related to each other by the carrier densities n and p . Therefore the unrenormalized band gap ϵ_g , which, of course, has to stay constant for all the spectra taken at different excitation intensities, and furthermore T_{eff} ,

$\mu^{\text{CB}}(T_{\text{eff}})$, and $\mu^{\text{VB}}(T_{\text{eff}})$ were used as independent plasma parameters.

The spectrum labeled $0.29I_0$ in Fig. 5 is characterized by $I_{\text{stim}}(\hbar\omega)/I_{\text{spont}}(\hbar\omega) \cong 2$ at $\hbar\omega=270.7 \text{ meV}$ ($\lambda=4.58 \mu\text{m}$), which indicates that this measurement was taken only slightly above the threshold of spontaneous emission. The most used absolute excitation intensity I_0 was estimated by measuring the laser output power and approximately determining the excited sample area. The result is $I_0 \cong 1.3 \text{ GW/m}^2$. This corresponds to a pulse energy per unit area of about 20 J/m^2 . The threshold of stimulated emission at $0.29I_0 \cong 0.38 \text{ GW/m}^2$ obtained in this way is consistent with the value determined from the measurement of the integrated photoluminescence intensity as a function of the excitation intensity (inset in Fig. 6). The line-shape fits to the photoluminescence spectra measured over the range $0.29 \leq I_{\text{exc}}/I_0 \leq 1.0$ directly yield the electron and hole densities. They grow with increasing excitation intensity, as shown in Fig. 7(a). Thereby the difference of the carrier densities of conduction and valence bands stays constant and corresponds to a hole concentration of $p_{\text{dop}} = (1.36 \pm 0.09) \times 10^{17} \text{ cm}^{-3}$ due to doping of the $x=0.041 \text{ Pb}_{1-x}\text{Eu}_x\text{Se}$ sample. The fact that this value is in excellent agreement with Hall data is an independent check for the validity of the calculations. Because of the increasing influence of exchange and correlation energy terms, the renormalized band gap $\epsilon_g + \Delta\epsilon_g$ is redshifted with increasing excitation intensity [see Fig. 7(b)], while the fits result in a single-particle band gap ϵ_g which is independent of the excitation level, as is expected: $\epsilon_g = (274.3 \pm 0.2) \text{ meV}$.

Another independent check of the results of line-shape fitting is provided by transmission magnetospectroscopy performed at $T_L=1.7 \text{ K}$ with very low radiation powers. Extrapolation of the measured transition energies between Landau levels yielded an energy gap of 273.4 meV . This value is about 0.9 meV smaller than ϵ_g , the

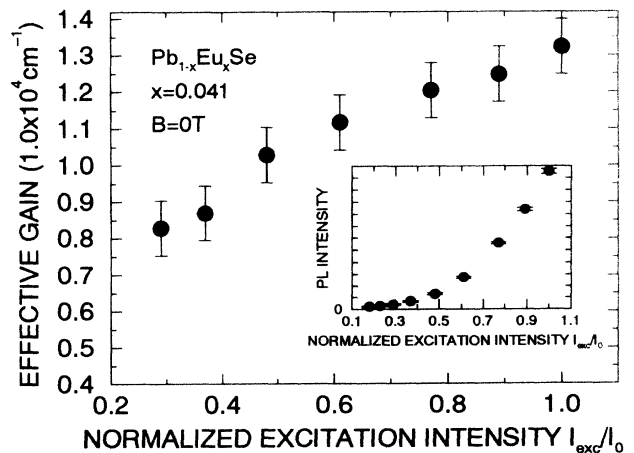


FIG. 6. Effective net optical gain as a function of excitation intensity, for the spectra given in Fig. 5. Inset: integrated photoluminescence intensity as a function of excitation intensity. The onset of stimulated emission at about $0.3I_0$ is clearly seen.

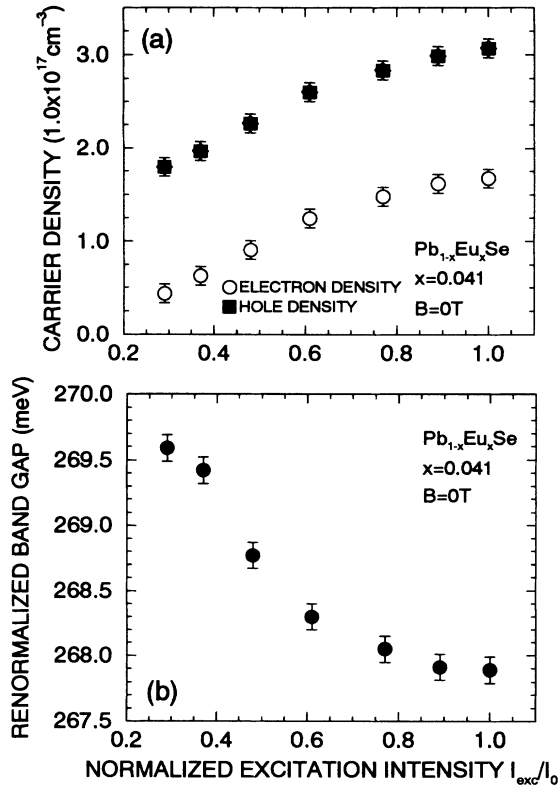


FIG. 7. (a) Electron and hole densities as functions of excitation intensity. (b) Renormalized band gap as a function of excitation intensity.

difference being due to the band-gap renormalization by doping using $p_{\text{dop}} = (1.36 \pm 0.09) \times 10^{17} \text{ cm}^{-3}$, Eq. (18) results in $\Delta\epsilon_g = -1.3 \text{ meV}$, in fairly good agreement with the observed difference. Comparison of this value with Fig. 1 additionally demonstrates that the $\epsilon_{r,0}$ approximation (including the polaron shift) cannot apply for our system since it yields $\Delta\epsilon_g \cong -10 \text{ meV}$ instead of about 1 meV as observed. The renormalized band gap plotted versus the excitation intensity in Fig. 7(b) nearly corresponds to the low-energy tail of the luminescence lines (see Fig. 5). If one assumes this to be the single-particle fundamental gap, the error is about 5 meV even at the lowest excitation intensity where spectra with acceptable signal-to-noise ratio are obtainable.

Spatial inhomogeneities in the electron-hole plasma

Calculating the carrier-density dependent part of the self-energy by considering the exchange and correlation energy terms only according to Eq. (18), but not taking into account the additional energy terms given in Eq. (19), the fit to the photoluminescence lines results in a smaller unrenormalized band gap than observed by magnetotransmission. If electron-hole correlations are assumed to result in small corrections to the exchange energy terms,⁷ just as are known for electron-electron and hole-hole correlations [see Eqs. (16) and (17)], then the above-mentioned underestimation of $\Delta\epsilon_g$ has to be taken as a hint of spatial inhomogeneities in the electron-hole

plasma because of spatially inhomogeneous excitation. The large Fermi pressures which accompany such an experimental situation may cause an expansion of the electron-hole plasma, and therefore be responsible for the observed saturation of the plasma density and of the corresponding band-gap renormalization at high excitation intensities [see Figs. 7(a) and 7(b)].³⁹

However, these spatial inhomogeneities of an electron-hole plasma (EHP) in direct-band-gap semiconductors are not to be mixed up with the phase separation and the corresponding formation of electron-hole droplets [electron-hole liquid (EHL)] known to occur in indirect-band-gap semiconductors. The Hartree-Fock energy plotted in Fig. 1 shows a shallow minimum with a depth of about 0.14 meV $\cong 1.6 \text{ K}$ at an electron density of $n_0 \cong 1 \times 10^{15}$ (inset in Fig. 1). However, due to the very small lifetimes of photoexcited carriers in direct-band-gap semiconductors, due to the usual high doping carrier concentrations of IV-VI compounds and due to the experimental conditions applied when performing the photoluminescence measurements ($T_L \geq 1.7 \text{ K}$; densities of the photoexcited carriers in the range of $\approx 10^{16}$ to $\approx 10^{18} \text{ cm}^{-3}$), an equilibrium situation according to the minimum shown in the inset of Fig. 1 will never be observable in IV-VI semiconductors.

Whereas in the case of an EHL one expects the sum $\epsilon_g + \Delta\epsilon_g + \mu^{\text{CB}}(T_{\text{eff}}) + |\mu^{\text{VB}}(T_{\text{eff}})|$, and the sum of the quasi-Fermi levels $\mu^{\text{CB}}(T_{\text{eff}}) + |\mu^{\text{VB}}(T_{\text{eff}})|$ also, to remain constant if the excitation intensity I_{exc} is increased,^{39,40} the growth of these quantities as it results from our photoluminescence spectra is characteristic of an electron-hole plasma in the absence of any phase separation [see Fig. 8(a)].

Also, the observed increase of the effective carrier temperature with the increasing sum of electron and hole densities, as shown in Fig. 8(b), is understood in terms of an expanding plasma. In contrast, the density of an EHL should slightly decrease with increasing effective temperature.^{39,40}

B. Photoluminescence in external magnetic fields

A possible influence of an external magnetic field on many-particle interactions has been investigated by measuring the photoluminescence of another p -type $\text{Pb}_{1-x}\text{Eu}_x\text{Se}$ sample ($x=0.039$), which was selected because its band structure in a magnetic field has been very carefully determined by CARS (coherent anti-Stokes Raman scattering) and transmission magnetospectroscopy. The corresponding photoluminescence measurements were performed at $T_L = 1.7 \text{ K}$ in Faraday geometry. A quite high but constant excitation intensity I_{exc} was used to make band-gap renormalization effects as large as possible. Because of the anisotropy of the energy bands the sample surface must be aligned carefully perpendicular to the magnetic-field direction. The aperture of the magnet then enforced a perpendicular incidence of the exciting laser beam and detection of the photoluminescence light. In this case a forward geometry was preferred. Typical spectra are shown in Fig. 9. The observed magnetic-field dependence of the recombination radiation maximum is

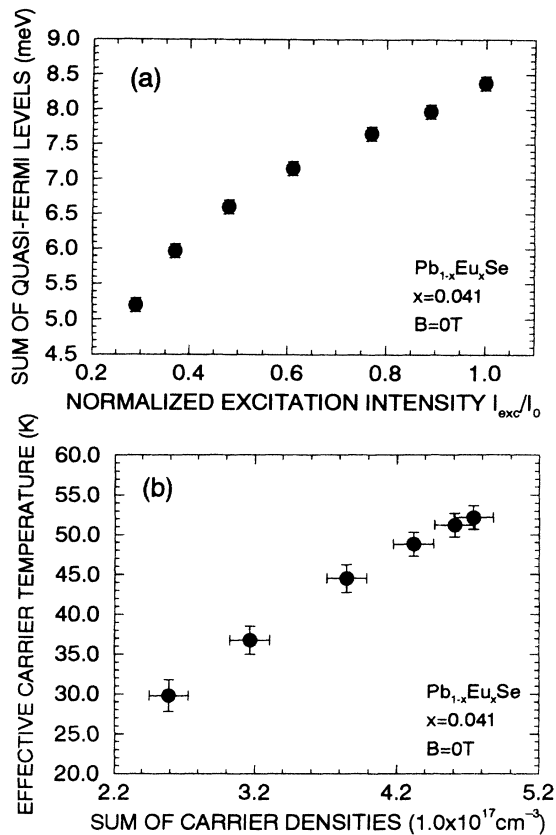


FIG. 8. (a) Sum of quasi-Fermi levels as a function of excitation intensity. (b) Effective carrier temperature as a function of the sum of electron and hole densities.

not in agreement with the wavelength shift of the lowest interband transition between Landau levels, $O_{\text{CB}}^+ \rightarrow O_{\text{VB}}^-$ ($\Phi = 70.53^\circ$). Particularly for high magnetic field this should be the dominating transition. This contradiction clearly demonstrates the need for the theoretical models developed in Secs. III and IV of this paper. Furthermore, the decrease of the half-widths of the photoluminescence lines with increasing magnetic field can only be explained if a line-shape analysis is used for the interpretation of the experimental data.

The spectra shown in Fig. 9 can be perfectly fitted to theoretical line shapes in the case of purely stimulated emission (due to high excitation levels) calculated from k -conserving (k_B conserving, respectively) interband transitions.

Thereby it turns out that the respective maximum of the recombination radiation is *not* caused by that interband transition with the lowest quantum energy $\hbar\omega$ being allowed according to the selection rules given in Table II. In contrast, one has to consider explicitly the combined density of states and the occupation probabilities of the levels of both bands in order to relate the observed maxima of the luminescence intensity to the corresponding Landau levels of the conduction and valence bands (see Fig. 4).

The photoluminescence spectra shown in Fig. 9 obviously shift toward shorter wavelength with increasing

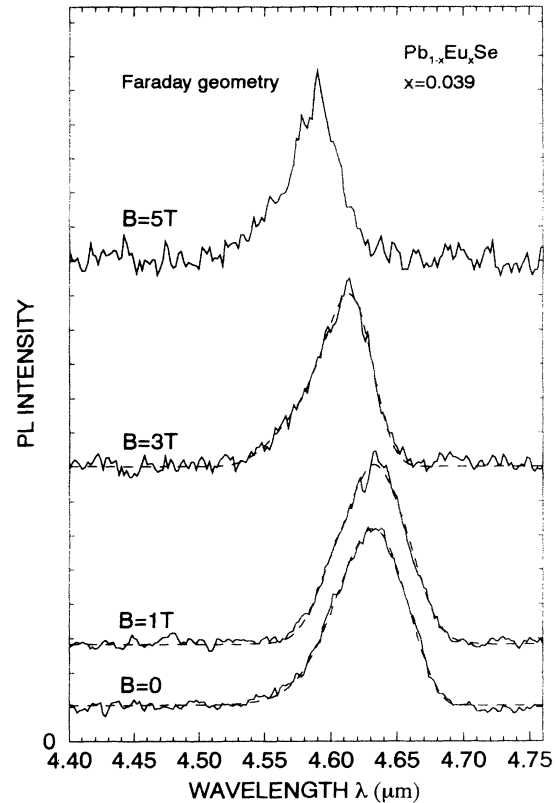


FIG. 9. Photoluminescence spectra at different magnetic fields. Broken lines: calculated line shapes (see text; parameters as plotted in Figs. 10 and 11, respectively).

magnetic field. However, the observed blueshift is smaller than expected according to the well-known energy band structure of the sample. Thus the value of the renormalized band gap at zero magnetic field $\varepsilon_g + \Delta\varepsilon_g$, which is the energy reference for the calculation of the Landau fans and which occurs in the expression of the absorption constant [Eq. (30)] and therefore also in the corresponding one of the macroscopic emission rate, has to be lowered with increasing magnetic-field strength. Thus there must be a magnetic-field dependence of the band-gap renormalization, that means a redshift of $\varepsilon_g + \Delta\varepsilon_g$ as a function of B , as shown in Fig. 10(a). The full line is calculated after Ref. 28, and demonstrates that the proportionality of the exchange energies to $B^{1/3}$ is very well fulfilled in our experimental situation.

Generally, one expects an increase of the electron and hole densities to accompany an increase of exchange and correlation energy terms. Therefore, by means of the obtained values for the fit parameters T_{eff} , $\mu^{\text{CB}}(B, T_{\text{eff}})$, $\mu^{\text{VB}}(B, T_{\text{eff}})$, and τ_g , the carrier densities were calculated under consideration of the cutoff energies Eqs. (10) and (11). As a result, at constant excitation intensity (with $\hbar\omega_L \gg \varepsilon_g$) the plasma density increases with increasing magnetic-field strength [see Fig. 10(b)]. The difference of electron and hole densities, however, stays constant and corresponds to a hole concentration of $p_{\text{dop}} = (1.48 \pm 0.09) \times 10^{17} \text{cm}^{-3}$ due to doping. The line-shape fits result in comparatively high values for the net

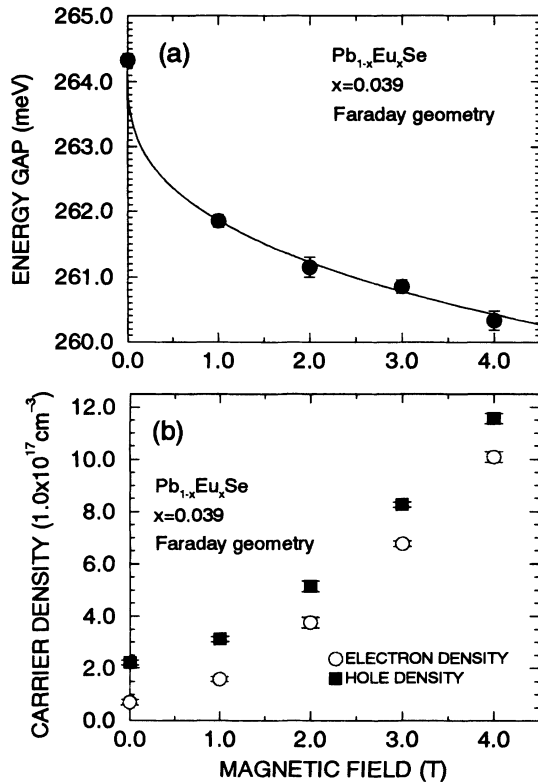


FIG. 10. (a) Band-gap renormalization as a function of magnetic field. (b) Carrier densities as a function of magnetic field (constant excitation).

optical gain g , even at small magnetic-field strengths B . In addition, the increase of g as well as the corresponding increase of the plasma density $n+p$ with increasing B is strongly nonlinear. Therefore, an influence of resonator and saturation effects on the photoluminescence spectra measured for very high magnetic fields cannot be excluded. In fact, the spectra for $B \geq 5T$ could not be fitted satisfactorily by the model described in the theoretical sections, neglecting resonator and saturation effects. As pointed out above, for $B \neq 0$ resonator effects from experimental reasons could not be avoided by tilting the sample with respect to the direction of propagation of the radiation, as was possible for $B = 0$.

As discussed above by means of the line-shape analysis of the $B = 0$ photoluminescence spectra, the increase of the effective carrier temperature T_{eff} with increasing magnetic-field strength B , and accordingly with increasing plasma density $n+p$ as shown in Figs. 11(a) and 11(b), clearly indicates the experimental observation of a homogeneous electron-hole plasma without formation of droplets in the direct-band-gap semiconductor $\text{Pb}_{1-x}\text{Eu}_x\text{Se}$.

VI. CONCLUSIONS

The photoluminescence spectra of narrow-gap IV-VI epitaxial films can be described in most cases by a line-

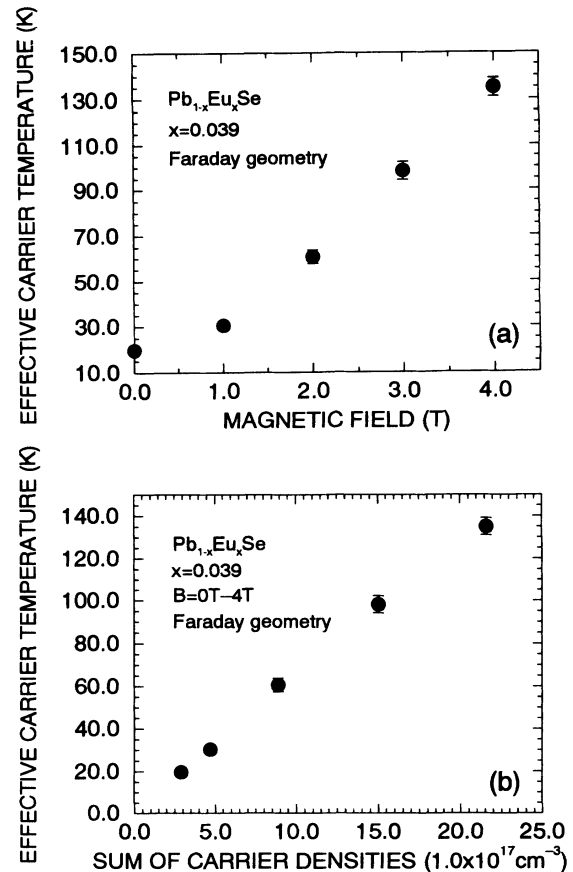


FIG. 11. (a) Effective carrier temperature as a function of magnetic field. (b) Effective carrier temperature as a function of the sum of electron and hole densities.

shape model which is based on \mathbf{k} -conserving interband transitions. Only in a few samples (probably with high impurity concentrations) and with special experimental situations (low excitation, high magnetic fields) the model which assumes violation of the \mathbf{k} -selection rule allows better fits to the experimental data.

All the observed spectra were due to a superposition of stimulated and spontaneous emission. Even at the lowest excitation level, where an acceptable signal-to-noise ratio was achieved, the amount of stimulated emission was considerable.

Despite the high dielectric constants of the IV-VI compounds, many-particle effects have to be taken into account. The observed band-gap renormalization at $B = 0$ is in agreement with the $\epsilon_{r,\infty}$ approximation, which neglects the polaron shift of the band gap and calculates exchange and correlation energy terms using the high-frequency dielectric constant. In an external magnetic field the band-gap renormalization increases proportional to $B^{1/3}$.

Keeping the excitation intensity constant, the density of photoexcited carriers as well as their effective temperature increases with magnetic field.

All these results were obtained using samples with very

well-known energy-band structures.

It turned out that the description of the electron-hole plasma and the fact that pure spontaneous emission could not be observed needs a high number of plasma parameters. Thus it seems difficult to determine band parameters like one-particle energy gaps or effective masses from photoluminescence experiments without additional information.

ACKNOWLEDGMENTS

Very helpful discussions with G. Bauer are gratefully acknowledged. Samples were given by M. Tacke, G. Springholz, and N. Frank. We thank W. Hofmann, G. Grادل, and U. Fichtel for making unpublished data available. The project was financially supported by Emil-Warburg Foundation.

- ¹W. C. Goltsos, A. V. Nurmikko, and D. L. Partin, *Solid State Commun.* **59**, 183 (1986).
- ²I. I. Zasavitskii, L. Kowalczyk, B. N. Matsonasvilli, and A. V. Sazonov, *Fiz. Tekh. Polopruvoda.* **22**, 2118 (1988) [*Sov. Phys. Semicond.* **22**, 1338 (1988)].
- ³J. W. Tomm, K. H. Herrmann, H. Böttner, M. Tacke, and A. Lambrecht, *Phys. Status Solidi A* **119**, 711 (1990).
- ⁴J. W. Tomm, K. H. Herrmann, and A. E. Yunovich, *Phys. Status Solidi A* **122**, 11 (1990).
- ⁵L. Kowalczyk, *Semicond. Sci. Technol.* **6**, 115 (1991).
- ⁶Y. A. Pokrovskii, *Phys. Status Solidi A* **11**, 385 (1972).
- ⁷G. Beni and T. M. Rice, *Phys. Rev. B* **18**, 768 (1978).
- ⁸T. M. Rice, in *Solid State Physics*, edited by H. Ehrenreich, F. Seitz, and D. Turnbull (Academic, New York, 1977), Vol. 32, p. 1ff.
- ⁹E. Göbel, H. Herzog, and M. H. Pilkuhn, *Solid State Commun.* **13**, 719 (1973).
- ¹⁰G. Göbel, *Appl. Phys. Lett.* **24**, 492 (1974).
- ¹¹E. O. Göbel, O. Hildebrand, and K. Löhnert, *IEEE J. Quantum Electron.* **13**, 848 (1977).
- ¹²E. O. Göbel and G. Mahler, *Festkörperprobleme Advances in Solid State Physics*, edited by J. Treusch (Vieweg, Braunschweig, 1979), Vol. XIX, p. 105.
- ¹³R. Dalven in *Solid State Physics*, edited by H. Ehrenreich, F. Seitz, and D. Turnbull (Academic, New York, 1973), Vol. 28, p. 179.
- ¹⁴M. Adler, C. Hewes, and S. Senturia, *Phys. Rev. B* **7**, 5186 (1973).
- ¹⁵G. Bauer, H. Pascher, and W. Zawadzki, *Semicond. Sci. Technol.* **7**, 703 (1992).
- ¹⁶D. Mitchell and F. Wallis, *Phys. Rev.* **151**, 581 (1966).
- ¹⁷R. B. Dingle, *Proc. R. Soc. London Ser. A* **211**, 517 (1952).
- ¹⁸L. M. Roth and P. N. Argyres, in *Semiconductors and Semimetals*, edited by R. K. Willardson and A. C. Beer (Academic, New York, 1966), Vol. 1, p. 159.
- ¹⁹W. Götze and J. Hajdu, *J. Phys. C* **11**, 3993 (1978).
- ²⁰M. Rösler and R. Zimmermann, *Phys. Status Solidi B* **67**, 525 (1975).
- ²¹T. M. Rice, *Nuovo Cimento B* **23**, 226 (1974).
- ²²M. Combescot and P. Nozieres, *J. Phys. C* **5**, 2396 (1972).
- ²³M. Gell-Mann and K. A. Brueckner, *Phys. Rev.* **106**, 364 (1957).
- ²⁴D. Pines, *Elementary Excitations in Solids* (Benjamin, New York, 1964), p. 65ff.
- ²⁵G. Beni and T. M. Rice, *Phys. Rev. Lett.* **37**, 874 (1976).
- ²⁶M. Rösler and R. Zimmermann, *Phys. Status Solidi B* **83**, 85 (1977).
- ²⁷L. V. Keldysh and A. P. Silin, *Zh. Eksp. Teor. Fiz.* **69**, 1053 (1975) [*Sov. Phys. JETP* **42**, 535 (1975)].
- ²⁸S. T. Chui, *Phys. Rev. B* **8**, 3438 (1974).
- ²⁹Y. E. Pokrovskii and V. B. Timofeev, in *Physics Reviews*, edited by I. M. Khalatnikov (Soviet Scientific Reviews, Moscow, 1979), Vol. 1, p. 191.
- ³⁰G. Lasher and F. Stern, *Phys. Rev. A* **133**, 533 (1964).
- ³¹F. Stern, in *Solid State Physics*, edited by F. Seitz and D. Turnbull (Academic, New York, 1963), Vol. 15, p. 364.
- ³²W. W. Anderson, *IEEE J. Quantum Electron.* **13**, 532 (1977).
- ³³L. M. Roth, B. Lax, and S. Zwerdling, *Phys. Rev.* **114**, 90 (1959).
- ³⁴R. Grisar, H. Burkhard, G. Bauer, and W. Zawadzki, in *Proceedings of the International Conference on Narrow Gap Semiconductors*, edited by Rauluskiewicz (PWN, Warszawa, 1978), p. 405.
- ³⁵K. L. Shaklee, R. E. Nahory, and R. F. Leheny, *J. Lumin.* **7**, 284 (1973).
- ³⁶P. Norton and M. Tacke, *J. Cryst. Growth* **81**, 405 (1987).
- ³⁷A. Lambrecht, N. Herres, B. Spanger, S. Kuhn, H. Böttner, M. Tacke, and J. Evers, *J. Cryst. Growth* **108**, 301 (1991).
- ³⁸K. Bohnert, M. Anselment, G. Kobbe, C. Klingshirn, H. Haug, S. W. Koch, S. Schmitt-Rink, and F. F. Abraham, *Z. Phys. B* **42**, 1 (1981).
- ³⁹M. Gal, Y. Hefetz, J. K. Ajo, and A. V. Nurmikko, *Phys. Rev. B* **28**, 4500 (1983).
- ⁴⁰O. Hildebrand, E. O. Goebel, K. M. Romanek, H. Weber, and G. Mahler, *Phys. Rev. B* **17**, 4775 (1978).